Unified explanation for optical and electron paramagnetic resonance spectra of Cr^{3+} ions in $LiNbO_3$ crystals

1997 J. Phys.: Condens. Matter 9 529

(http://iopscience.iop.org/0953-8984/9/2/020)

J. Phys.: Condens. Matter **9** (1997) 529–539. Printed in the UK PII: S0953-8984(97)74521-1

Unified explanation for optical and electron paramagnetic resonance spectra of Cr^{3+} ions in $LiNbO_3$ crystals

M G Zhao and Y Lei

Institute of Solid State Physics, Sichuan Normal University, Chengdu 610068, People's Republic of China

Received 15 May 1996, in final form 23 August 1996

Abstract. An approximately microscopic model is developed for the Cr^{3+}–$6O^{2-}$ cluster and applied to study the optical data and electron paramagnetic resonance (EPR) g-factors and the zero-field splitting D-value in $LiNbO_3$:Cr^{3+}. Analysis of the optical and EPR data indicate that Cr^{3+} ions substitute at Nb sites and Nb-vacancy (Li) sites simultaneously. The results are in good agreement with the experimental findings. This means that the optical and EPR data and the substitution site of Cr^{3+} ions in $LiNbO_3$ can be interpreted uniformly.

1. Introduction

Renewed interest in the spectroscopy of transition-metal ions in $LiNbO_3$ crystals follows from applications in electro-optics and laser technology [1–13]. In the ferroelectric phase, the Li and Nb ions are surrounded by six oxygen atoms in a distorted octahedron and lie along the C_3 axis but away from the centre of the octahedron. In the [111] direction, the cations are distributed in the octahedron in the following sequence: Nb, structure vacancy, Li, Nb, structure vacancy, Li, etc [13]. In general, Cr^{3+} ions can be situated at either the Li^+ or the Nb^{5+} site [3]. Earlier, Glass [12] conducted a comparative study of the absorption and fluorescence spectra of $LiNbO_3$:Cr^{3+} and concluded that Cr^{3+} substituted at the Nb site and not the Li site. By ENDOR it is shown that the EPR signal is due to Cr^{3+}, which substitutes for Nb [5]. Recently, Cr^{3+} substituted at both Nb and other sites (possibly Li sites) was obtained from axial EPR spectra [14, 15] and also from the fluorescence studies of R lines of Cr^{3+} ions [2, 10, 11]. Martin *et al* [1] maintained that the main axial EPR spectra and optical spectroscopy arise from the Cr^{3+} ion at the Nb site. However, at the present time there is no satisfactory and quantitative unified explanation for the absorption and fluorescence spectra, and the electron paramagnetic resonance (EPR) g-factors and zero-field splitting D-value of $3d^3$ ions in crystals. In this work, we try to develop a quantitative unified explanation for the spectroscopic behaviours and the substitution site of Cr^{3+} ions in $LiNbO_3$:Cr^{3+} single crystals. The calculated results agree well with the experimental findings.

2. Invalidity of the high-order perturbation formula for the splitting of the R line

Following the work by Macfarlane [16], the splitting of the R line was given by

0953-8984/97/020529+11$19.50

$$\delta_R = E(^2E, R_2) - E(^2E, R_1) = V\zeta_d[-4/3D_7 - 16B/D_7D_{13} + 4B/D_7D_{12} - 16B/D_{10}D_{12} + 4B/D_{10}D_{13}] + V'\zeta_d[8\sqrt{2}B/D_7D_{12} - 2\sqrt{6}B/D_7D_{13} - 2\sqrt{2}B/D_3D_{12} - 2\sqrt{2}B/D_3D_{13}] \tag{1}$$

with

$$D_2 = 15B + 5C \qquad D_3 = 10Dq + 9B + 3C$$
$$D_7 = 10Dq + 6B \qquad D_{10} = 10Dq \tag{2}$$
$$D_{12} = 10Dq + 14B + 3C \qquad D_{13} = 10Dq + 5B.$$

Using equations (1) and (2), the following result is obtained:

$$\delta_R = -5.17 \text{ cm}^{-1} \tag{3}$$

when

$$B = 785.7 \text{ cm}^{-1} \qquad C = 2839.4 \text{ cm}^{-1} \qquad Dq = 1445 \text{ cm}^{-1}$$
$$\zeta_d = 233.66 \text{ cm}^{-1} \qquad v = 25.8 \text{ cm}^{-1} \qquad V' = 900 \text{ cm}^{-1}. \tag{4}$$

However, using the complete energy matrices with C'_{3v} symmetry [16] and exactly diagonalizing them, we obtain

$$\delta_R = -35 \text{ cm}^{-1}. \tag{5}$$

This means that the high-order perturbation formula for δ_R is inadequate. Thus the previous calculation [12] is questionable because an unreasonable approximation was used in the calculation.

3. Complete diagonalization procedure for $3d^3$ and $3d^7$ ions in the C_{3v} symmetry field

The Hamiltonian including the electron–electron repulsions, the spin–orbit interactions and the crystal-field interactions is given by

$$H = H_e + H_{so} + H_{cf} \tag{6}$$

where

$$H_e = \sum_i \left(\frac{-\hbar^2}{2m} \nabla_1^2 - \frac{ze^2}{r_i} \right) + \sum_{i>j} \frac{e^2}{r_{ij}} \tag{7}$$

$$H_{so} = \sum_i \zeta_d \boldsymbol{S}(i) \cdot \boldsymbol{L}(i) \tag{8}$$

$$H_{cf} = \sum_{k,q,i} B_{kq} C_q^{(k)}(i). \tag{9}$$

The B_{kq} appearing in equation (9) are the crystal-field parameters and $C_q^{(k)}$ is the tensor harmonics. All other symbols appearing in equations (7) and (8) have their usual meanings.

In the intermediate-field coupling case, $H_e + H_{cf}$ is applied before the spin–orbit interactions. The matrix (120×120) for the combined Coulomb, crystal-field and spin–orbit interactions may be computer-generated similar to the earlier work [16–21].

In order to analyse the EPR spectrum the spin Hamiltonian (SH) for the axial symmetry case about a threefold axis was used. This was given by [22]

$$H_s = \beta(g_\parallel H_z S_z + g_\perp H_x S_x + g_\perp H_y S_y) + D S_z^2. \tag{10}$$

The symbols appearing in equation (10) have their usual meanings.

The coordinate system is chosen such that the z axis coincides with the symmetric axis C_3. The SH matrix elements are calculated in terms of the effective spin vectors. The spin ground state of the $3d^3$ configuration in crystal is the admixture of $S = 3/2$ and 1/2 spin states. In the effective SH formalism, the 'spin' is described by an effective spin s'.

By means of the approximate equivalence between the SH and complete diagonalization procedure (CDP), the following expressions are obtained:

$$2D = E(\pm 3/2)(\mathrm{CDP}) - E(\pm 1/2)(\mathrm{CDP}) \qquad (H = 0) \tag{11}$$

$$g_{\parallel} = \langle 3/2, 1/2|kL_z + 2.0023S_z|3/2, 1/2\rangle - \langle 3/2, -1/2|kL_z + 2.0023S_z|3/2, -1/2\rangle \tag{12a}$$

$$g_{\parallel} = (1/3)[\langle 3/2, 3/2|kL_z + 2.0023S_z|3/2, 3/2\rangle - \langle 3/2, -3/2|kL_z + 2.0023S_z|3/2, -3/2\rangle] \tag{12b}$$

$$g_{\perp} = \frac{2}{\sqrt{3}}\langle 3/2, 3/2|kL_x + 2.0023S_x|3/2, 1/2\rangle \tag{13a}$$

$$g_{\perp} = \langle 3/2, 1/2|kL_x + 2.0023S_x|3/2, -1/2\rangle. \tag{13b}$$

Here $E(3/2, \pm 3/2)$ and $E(3/2, \pm 1/2)$ denote the zero-field ($\boldsymbol{H} = \boldsymbol{0}$) eigenenergies of eigenstates $|3/2, \pm 3/2\rangle(\mathrm{CDP})$ and $|3/2, \pm 1/2\rangle(\mathrm{CDP})$, respectively, k is the orbit reduction factor and $k\boldsymbol{L} + 2.0023\boldsymbol{S}$ is the Zeeman magnetic moment operator; its matrices (120×120) may be computer generated; $k\boldsymbol{L} + 2.0023\boldsymbol{S} = \sum_i [k\boldsymbol{L}(i) + 2.0023\boldsymbol{S}(i)]$.

4. An approximately equivalent self-consistent-field molecular orbital model for Cr^{3+} ions in crystals

In the generalized crystal-field-like model, the C_{3v} crystal-field parameters B_{kq} were given by [20, 21]

$$B_{20} = -3e^2\langle r^2\rangle \sum_{i=1}^{2} \frac{3\cos^2\theta_i - 1}{R_i^3} \tag{14}$$

$$B_{40} = \frac{-3e^2\langle r^4\rangle}{4} \sum_{i=1}^{2} \frac{35\cos^4\theta_i - 30\cos^2\theta_i + 3}{R_i^5} \tag{15}$$

$$B_{43} = -B_{4-3} = [(\sqrt{35})3e^2\langle r^4\rangle/2][\sin^3\theta_2\cos\theta_2/R_2^5) - (\sin^3\theta_1\cos\theta_1/R_1^5)] \tag{16}$$

where the effective charge equals the valence charge which is $2e$ for O^{2-} ligands. The crystal-field parameters B_{kq} can be calculated from the structure data provided that the expectation values $\langle r^n\rangle$ are known. Consideration of the overlap between the central metal ion and the ligand orbitals, a reasonable approximation for the electrostatic parameters B and C, the spin–orbit constant ζ_d, the expectation values $\langle r^n\rangle$ and the orbit reduction factor k in crystal was made [20, 21]:

$$\begin{aligned} &B = N^4B_0 \qquad C = N^4C_0 \\ &\zeta_d = N^2\zeta_d^0 \qquad \langle r^n\rangle = N^2\langle r^n\rangle_0 \qquad K = N^2 \end{aligned} \tag{17}$$

where N is the average reduction factor due to the covalency, B_0 and C_0 are the electrostatic parameters, ζ_d^0 is the spin–orbit coupling constant and $\langle r^n\rangle_0$ is the expectation value of r^n in the free-ion state. As one can see, this model leaves at most one model parameter N, which remains to be determined from an experimentally or theoretically known energy level [20, 21].

For the Cr^{3+} ion, the parametrized d orbital is given by

$$R_d(r) = 0.5981\left(\frac{(2\zeta_1)^7}{6!}\right)^{1/2} r^2 \exp\left(-\frac{\zeta_1 r}{a_0}\right) + 0.6000\left(\frac{(2\zeta_2)^7}{6!}\right)^{1/2} r^2 \exp\left(-\frac{\zeta_2 r}{a_0}\right) \tag{18}$$

(the Bohr radius $a_0 = 0.529\,18$ Å $= 1$ au; ζ_1 and ζ_2 are Slater exponents) where $\zeta_1 = 4.739\,811\,418$ and $\zeta_2 = 1.648\,630\,058$.

From equation (18), we find that

$$\begin{aligned} &B_0 = 927\ \text{cm}^{-1}(\text{observed, } 927\ \text{cm}^{-1}; \text{SCF, } 808\ \text{cm}^{-1}[24]) \\ &C_0 = 3350\ \text{cm}^{-1}(\text{observed, } 3350\ \text{cm}^{-1}; \text{SCF, } 3336\ \text{cm}^{-1}[24]) \\ &\zeta_d^0 = 253.8\ \text{cm}^{-1}(\text{observed, } 270\ \text{cm}^{-1}; \text{SCF, } 273\ \text{cm}^{-1}[22]) \\ &\langle r^2\rangle_0 = 2.463\,95a_0^2 \\ &\langle r^4\rangle_0 = 16.4276a_0^4. \end{aligned} \tag{19}$$

The comparison of theory with experiment is shown in table 1.

Table 1. Spectrum of free Cr^{3+} ion.

		Energy levels (cm^{-1})	
Term	J	Theoretical value[c]	Experimental value[a,b]
^4F	3/2	0	0[a]
	5/2	219	235.8[a]
	7/2	518.3	555.6[a]
	9/2	891.3	945.6[a]
^4P	1/2	13 544	14 059[a], 13 640[b]
	3/2	13 638	14 177.1[a]
	5/2	13 895	14 471.3[a]
^2G	7/2	14 871	15 051.8[a], 14 660[b]
	9/2	15 191	15 401.6[a]
^2P	3/2	18 378	19 438.6[a], 18 400[b]
	1/2	18 499	19 519.2[a]
$^2D_2$	3/2	20 229	20 649.9[a], 19 930[b]
	5/2	20 278	20 664.3[a]
^2H	9/2	20 473	21 065.9[a], 20 590[b]
	11/2	20 500	21 320.7[a]
^2F	7/2	33 022	34 262.8[a]
	5/2	33 160	34 555.7[a]
$^2D_1$	5/2	50 974	52 975.3[a]
	3/2	51 143	53 152.0[a]

[a] From [25].
[b] From [26].
[c] Trees correction constant $\alpha_0 = 65\ \text{cm}^{-1}$; Racah correction constant $\beta_0 = -131\ \text{cm}^{-1}$.

We shall show in section 5 that our parametrized crystal-field-like model is approximately equivalent to the SCF DV–X_α method for Cr^{3+} ions in $LiNbO_3$.

5. Calculations and results

Since the Nb^{5+}–O^{2-} bond is stronger than the Li^+–O^{2-} bond, $LiNbO_3$ crystals have a tendency to non-stoichiometry with [Li]/[Nb] < 1. Such crystals therefore have a very

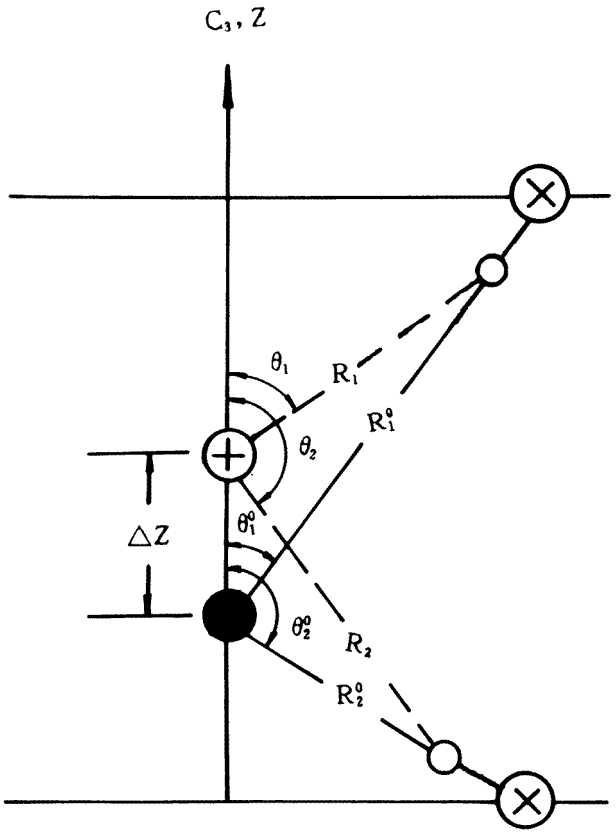

Figure 1. Distorted structure of Cr^{3+} site in $LiNbO_3$: ●, Nb^{5+}/Li^{+}; ⊕, Cr^{3+}; ⊗, O; ○, shifted O.

high concentration of intrinsic defects. O'Bryan *et al* [27] reported the composition ratio to be 48.45/51.55. Abraham and Marsh [28] reinvestigated the composition of $LiNbO_3$. The crystal structure was found to be given by $[Li_{1-5x}Nb_{5x}]Nb_{1-x}O_3$ with $x = 0.0118$, indicating that there are 5.9% vacant Li sites. So, we believe that firstly there are two kinds of Nb site, namely the regular sites Nb(I), and the unusual sites Nb(II) perturbed by a close Li^{+} vacancy, and secondly Cr^{3+} ions substitute for both Nb^{5+}(I) ions and Nb^{5+}(II) ions in the trigonally relaxed octahedral sites; this leads to two types of R line: $(R_1, R_2)(Cr^{3+}(I))$ and $(R_1, R_2)(Cr^{3+}(II))$ lines [2, 10, 11].

Following the experimental work by Abraham *et al* [13, 28, 29] and Glass [12], to within the range of experimental errors ($\Delta R_i = \pm 0.01$ Å; $\Delta\theta_i = \pm 1^\circ$), the structure data of Li^{+} and Nb^{5+} sites in the host $LiNbO_3$ crystal may be taken as, for the Li^{+} site (C_{3v} approximation),

$$\begin{aligned} &R_1^0 = 2.238 \text{ Å} \qquad R_2^0 = 2.068 \text{ Å} \\ &\theta_1 = 44.57^\circ \qquad \theta_2 = 110.26^\circ \end{aligned} \tag{20}$$

and, for the Nb^{5+} site (C_{3v} approximation),

$$\begin{aligned} &R_1^0 = 1.889\ \text{Å} \qquad R_2^0 = 2.112\ \text{Å} \\ &\theta_1 = 61.65^\circ \qquad \theta_2 = 133^\circ. \end{aligned} \tag{21}$$

Taking into account the local relaxation around the Cr^{3+} site as depicted in figure 1, we define

$$\begin{aligned} &f = R_i/R_i^0 \qquad (i = 1, 2) \\ &\Delta Z = Z(Cr^{3+}) - Z(\text{Nb/Li}) \qquad (Z \| C_3) \end{aligned} \tag{22}$$

where f denotes the relaxation factor of the bond lengths, ΔZ is the relaxation displacement along the C_3 axis, R_i are relaxed bond lengths, R_i^0 are the unrelaxed bond lengths, $Z(Cr^{3+})$ is the relaxed Z coordinate of the Cr^{3+} ion and Z(Nb/Li) is the Z coordinate of the Nb/Li ion.

The values of ΔZ and f are dependent on both the crystal growth conditions and the doping levels of $LiNbO_3$:Cr^{3+}.

Recently, Qiu [37] calculated the electronic structure of Cr^{3+} ions in $LiNbO_3$ with the DV– X_α method and found that the average transition energies of the $^2E(G)$ state for Cr^{3+} ions at Nb and Li sites in $LiNbO_3$ are 13 836 cm^{-1} and 13 805 cm^{-1}, respectively. By means of the approximate average equivalence between the DV– X_α calculation and our generalized crystal-field model, one obtains $N = 0.9595$ for the Nb site, and $N = 0.9658$ for the Li site.

Utilizing equations (14)–(22) we obtain the crystal-field parameter B_{kq} as a function of f and ΔZ. By diagonalizing the 120×120 matrix and utilizing the equations (11)–(13), we obtain the crystal-field energy levels and EPR g-factor and D-value. The final results are shown in tables 2–4. Comparing the theoretical d–d transitions and EPR parameters with the experimental values, it can be seen that good agreement between theory and experiments is obtained, as the Cr^{3+} ion substitutes for both Nb^{5+}(I) and Nb^{5+}(II). It can also be seen from table 4 that the experimental EPR and optical spectra cannot be reproduced by placing the Cr^{3+} ion at the Li position.

6. Discussion and conclusion

(a) This, to our knowledge, is the first attempt at a unified explanation for optical and EPR data, and the substitution site of Cr^{3+} ions in $LiNbO_3$ crystals. The good agreement between theory and experiments shows that the method and model are reasonable. In this scheme, there is no adjustable model parameter since the parameter N has been obtained equivalently from the SCF DV–X_α calculation.

(b) It is well known that the Cr–O bond lengths and bond angles may differ from the host cation–anion values. In concentrated ruby, for instance, the Cr^{3+} ion has been found to be displaced from the host Al^{3+} ion site by 0.06 Å [31]. It is currently accepted that for impurities in solids the bond lengths R_i can be determined through the EXAFS technique. It may be applied to any kind of impurity. However, impurity concentrations of the order of 100 ppm may be difficult to see by EXAFS [30], while concentrations of the order of 1 ppm of some transition-metal ions can be detected through EPR. In addition, the bond lengths of transition-metal ions in crystals can also be determined from superhyperfine splitting (SHF) measurements [32, 34]. So, the values of ΔZ and f obtained for Cr^{3+} ions at Nb sites may be further compared by other methods (for instance EXAFS, ENDOR and SHF). In view of the good and systematic agreement between the theory and the optical and EPR experiments, the results are reasonable and safe [38]. (The slight discrepancies in

Table 2. Comparison between theory and experiments.

Calculated energy[a] (cm^{-1})				Observed energy (cm^{-1})
Nb(II) site C_{3v} approximation; structure parameters $\Delta Z = -0.026$ Å and $f = 0.9985$		Nb(I) site C_{3v} approximation structure parameters $\Delta Z = 0.012$ Å and $f = 0.9936$		
O_h	C'_{3v}	O_h	C'_{3v}	[2–4, 10, 11, 14, 15]
	$^4A_2(F)$ ground state		$^4A_2(F)$ ground state	
^2E	^2E { 13 692 13 756	^2E	^2E { 13 756 13 819 (main)	{ 13 687 (weak) 13 762 (main) { 13 762 13 812 [11]
$^4T_2$	^4E { 13 891 13 937 14 069 14 164, $\Delta_T = 340$	$^4T_2$	^4E { 14 106 14 149 14 228 14 313, $\Delta_T = 267$	15 300, 15 330 [12] 15 310 [10, 11] $E(^4A_1) - E(^4E) = \Delta_T$ $\approx$ 180–360 [11]
	$^4A_1$ { 14 333 14 379		$^4A_1$ { 14 436 14 495	13 645 [2]
$^2T_1$	$^2A_2$ 14 733	$^2T_1$	$^2A_2$ 14 682	
	^2E { 14 894 14 935		^2E { 14 968 14 986	14 050 14 630 [12]
$^2T_2$	^2E { 20 569 21 000	$^2T_2$	^2E { 20 558 20 564	19 300
	$^2A_1$ 21 109		$^2A_1$ 21 333	20 200 [12]
$^4T_1$	^4E { 20 545 20 742 20 841 20 877	$^4T_1$	^4E { 20 839 20 908 20 915 21 021	 20 850 [12] 20 833 [10]
	$^4A_2$ { 21 869 21 885		$^4A_2$ { 22 479 22 486	21 390 [12]
$^2T_2$	$^2A_1$ 25 749	$^2T_2$	$^2A_1$ 25 962	
	^2E { 27 887 27 944		^2E { 28 079 28 148	

EPR		EPR	
Calculated	Observed	Calculated	Observed
$D = -0.2031$	± 0.21 (weak) [14]	$D = -0.3999$ (main)	-0.393 [4] ± 0.411 (main) [14]
$g_\parallel = 1.960\,15$	1.96 [6]	$g_\parallel = 1.959\,63$	1.96 [6]
$g_\perp = 1.961\,22$	1.968 [14]	$g_\perp = 1.962\,44$	1.968 [14]
$\bar{g} = 1.960\,69$	1.97 [3, 4]	$\bar{g} = 1.961\,04$	1.97 [3, 4]

R lines		R lines	
Calculated	Observed	Calculated	Observed
13 692	13 687 (weak)	13 756	13 762
13 756	13 762 [11] (main)	13 819	13 812 [11] (main)
(For magnetic dipole transition see [35, 36])		(For magnetic dipole transition see [35, 36])	

[a] The Trees and Racah corrections were neglected.

the experimental D-values may be due to the different crystal growth conditions of $LiNbO_3$ or the fitting procedure used.)

Table 3. Comparison between theory and experiments.

Calculated energy[a] (cm^{-1})					
Nb(II) site C_{3v} approximation; structure parameters $\Delta Z = -0.026$ Å and $f = 0.9985$			Nb(I) site; C_{3v} approximation; structure parameters $\Delta Z = 0.0136$ Å and $f = 0.9980$		Observed energy (cm^{-1})
O_h	C'_{3v}		O_h	C'_{3v}	[2–4, 10, 11, 14, 15]
$^4A_2$(F) ground state			$^4A_2$(F) ground state		
^2E	^2E	13 692 13 756	^2E	^2E	13 619 13 681 (main)
					13 686 (weak) 13 754 (main)
					13 616 13 686 [2]
$^4T_2$	^4E	13 891 13 937 14 069 14 164, $\Delta_T = 340$	$^4T_2$	^4E	13 793 13 839 13 965 14 049, $\Delta_T = 331$
					15 300, 15 330 [12] 15 310 [10, 11] $E(^4A_1) - E(^4E) = \Delta_T$ $\approx$ 180–360 [11]
	$^4A_1$	14 333 14 379		$^4A_1$	14 228 14 258
					13 645 [2]
$^2T_1$	$^2A_2$	14 733	$^2T_1$	$^2A_2$	14 628
	^2E	14 894 14 935		^2E	14 936 14 964
					14 050 14 630 [12]
$^2T_2$	^2E	20 569 21 000	$^2T_2$	^2E	20 287 21 335
					19 300
	$^2A_1$	21 109		$^2A_1$	21 237
					20 200 [12]
$^4T_1$	^4E	20 545 20 742 20 841 20 877	$^4T_1$	^4E	20 471 20 528 20 647 20 824
					20 850 [12] 20 833 [10]
	$^4A_2$	21 869 21 885		$^4A_2$	22 098 22 111
					21 390 [12]
$^2T_2$	$^2A_1$	25 749	$^2T_2$	$^2A_1$	25 642
	^2E	27 887 27 944		^2E	27 761 27 830

EPR		EPR	
Calculated	Observed	Calculated	Observed
$D = -0.2031$	± 0.21 (weak) [14]	$D = -0.4097$ (main)	-0.393 [4] ± 0.411 (main) [14]
$g_\parallel = 1.960\,15$	1.96 [6]	$g_\parallel = 1.958\,59$	1.96 [6]
$g_\perp = 1.961\,22$	1.968 [14]	$g_\perp = 1.961\,54$	1.968 [14]
$\bar{g} = 1.960\,69$	1.97 [3, 4]	$\bar{g} = 1.960\,00$	1.97 [3, 4]

R lines		R lines	
Calculated	Observed	Calculated	Observed
13 692	13 686	13 619	13 616
13 756	13 754 [11] (weak)	13 681 (main)	13 686 [2] (main)
(For magnetic dipole transition see [35, 36])		(For magnetic dipole transition see [35, 36])	

[a] The Trees and Racah corrections were neglected.

(c) Qiu [37] has calculated five d–d transition energies for Cr^{3+} ions in $LiNbO_3$ with the DV– X_α method. He deduced a value of -817 cm^{-1} for the $^4T_2$ splitting Δ_T at the Nb site,

Table 4. Comparison between theory and experiments.

Calculated energy (cm^{-1})				Observed energy (cm^{-1})
Li site; $f = 0.70$ and $\Delta Z = 0.31$ Å		Li site; $f = 0.883$ and $\Delta Z = 0.213$ Å		
O_h	C_{3v}	O_h	C_{3v}	[2–4,10, 11, 14, 15])
$^4A_2$(F) ground state		$^4A_2$(F) ground state		
^2E	^2E { 15 182 15 246	^2E	^2E { 15 462 14 566	{ 13 687 { 13 762 13 762 { 13 812 [11] { 13 686 { 13 616 13 753 { 13 686 [2]
$^4T_2$	^4E { 72 364 72 408 72 451 72 492	$^4T_2$	^4E { 18 797 18 833 18 896 18 980	15 300, 15 330 [12] 15 310 [10, 11] $E(^4A_1) - E(^4E) = \Delta_T$ $\approx$ 180–360 [11]
	$^4A_1$ { 71 629 71 632		$^4A_1$ { 18 990 18 996	13 645 [2]
$^2T_1$	$^2A_2$ 15 624	$^2T_1$	$^2A_2$ 15 114	
	^2E { 15 885 15 899		^2E { 15 484 15 519	14 050 14 630
$^2T_2$	^2E { 25 176 25 205	$^2T_2$	^2E { 21 869 21 971	19 300
	$^2A_1$ 25 656		$^2A_1$ 22 736	20 200 [12]
$^4T_1$	^4E { 81 631 81 654 81 668 81 678	$^4T_1$	^4E { 26 385 26 410 26 433 26 457	 20 850 [12] 20 833 [10]
	$^4A_2$ { 81 347 81 358		$^4A_2$ { 27 690 27 695	21 390 [12]
$^2T_2$	$^2A_1$ 86 316	$^2T_2$	$^2A_1$ 30 899	
	^2E { 86 408 86 740		^2E { 33 278 33 432	
$D = -0.2018$		$D = -0.4089$		-0.393 [4] ± 0.411 (main), ± 0.21 (weak) [14] ± 0.39 [6] ± 0.45 [3]
$g_\parallel = 1.9935$ $g_\perp = 1.9941$ $\bar{g} = 1.9938$		$g_\parallel = 1.9687$ $g_\perp = 1.9717$ $\bar{g} = 1.972$		$\bar{g} = 1.96$ $\bar{g} = 1.968$ [14, 15] $\bar{g} = 1.970$
R-line splitting, 64 (For magnetic dipole transition, see [35,36])		R-line splitting, 4 (For magnetic dipole transition, see [35, 36])		75, 50 [11, 36] 70, 70 [2, 36]

which is essentially different from those of 267–331 cm^{-1} obtained by us (observed, 180–360 cm^{-1}). So, the so-called approximate equivalence between the generalized crystal-field-like model and the DV–X_α calculation is only an average energy equivalence instead of total equivalence. In addition, to our knowledge, the X_α calculation cannot quantitatively explain the EPR parameters D, $g_\parallel$ and $g_\perp$. Furthermore, it should be pointed out that we have obtained an average value of 13 904 cm^{-1} for the $^4T_2$ state of Cr^{3+} in the unrelaxed

Nb site ($\Delta Z = 0$; $f = 1$) in $LiNbO_3$, using $N = 0.9595$, which is in good agreement with the DV–X_α-value of 14 019 cm^{-1} [37]. It shows that $\langle r^4 \rangle_0 = 16.4276$ au is equivalently consistent with the MO calculation.

Acknowledgment

This work was supported by the National Natural Science Foundation of China (grant 19574036).

References

[1] Martin A, Lopez F J and Agullo-Lopez F 1992 *J. Phys.: Condens. Matter* **4** 847
[2] Jia W, Liu H, Knutson R and Yen W M 1990 *Phys. Rev.* B **41** 10 906
[3] Evlanova N F, Kornienko L S, Rashkovich L N and Rybaltovskii A O 1968 *Sov. Phys.–JETP* **26** 1090
[4] Grachev V G, Malovichko G I and Troitskii V V 1987 *Sov. Phys.–Solid State* **29** 349
[5] Schirmer O F, Thiomana O and Wohlecke M 1991 *J. Phys. Chem. Solids* **52** 185
[6] Siu G G and Zhao M G 1991 *Phys. Rev.* B **43** 13 575
[7] Zhong G, Jian J and Wu Z 1980 *Proc. 11th Int. Quantum Electronic Conf.* (New York: IEEE) p 361
[8] Kovcas L, Foldvari I, Gravero I and Polgar K 1988 *Phys. Lett.* **133A** 433
[9] Lifante G, Cusso F, Sanz-Garcia J A, Monteil A, Varrel B, Boulon G and Carcia J 1991 *Chem. Phys. Lett.* **176** 482
[10] Camarillo E, Tocho J, Vergara I, Diegues E, Carcia-Sole J and Jaque F 1992 *Phys. Rev.* B **45** 4600
[11] Camanillo E, Carcia-Sole J, Cusso F, Agullo-Lopez F, Sanz-Carcia J A, Han T P J, Jaque F H and Henderson B 1991 *Chem. Phys. Lett.* **185** 505
[12] Glass A M 1969 *J. Chem. Phys.* **50** 1501
[13] Abraham S C, Reddy J M and Bernstein J L 1966 *J. Phys. Chem. Solids* **27** 997
[14] Rexford D G, Kim Y M and Story H S 1970 *J. Chem. Phys.* **52** 860
[15] Park I W, Choh S H, Song K J and Kim J N 1993 *J. Korean Phys. Soc.* **26** 122
[16] Macfarlane R M 1970 *Phys. Rev.* B **1** 988; 1963 *J. Chem. Phys.* **39** 3118
[17] Konig E and Schnakig R 1976 *Phys. Status Solidi* b **77** 657
[18] Konig E and Kremer S 1977 *Ligand Field Energy Diagrams* (New York: Plenum)
[19] Febbraro S 1987 *J. Phys. C: Solid State Phys.* **20** 5367
[20] Zhao M G and Chiu M 1994 *Phys. Rev.* B **49** 12 556
[21] Zhao M G and Chiu M 1995 *Phys. Rev.* B **52** 10 043
[22] Abragam A and Bleaney B 1970 *Electron paramagnetic Resonance of Transition Metal Ions* (Oxford: Clarendon)
[23] Rosseinski D R and Dorrity I A 1978 *Coord. Chem. Rev.* **25** 31
[24] Van Der Laan G 1991 *J. Phys.: Condens. Matter* **3** 7443
[25] Ekberg O 1973 *Phys. Scr.* **7** 55
[26] Moore C E 1952 *Atomic Energy Levels* NBS Circular 467 (Washington, DC: US Government Printing Office)
[27] O'Bryan H M, Gallagher P K and Brandle C D 1985 *J. Am. Ceram. Soc.* **68** 493
[28] Abraham S C and Marsh P 1986 *Acta Crystallogr.* B **42** 61
[29] Abraham S C, Hamilton W C and Reddy J M 1966 *J. Phys. Chem. Solids* **27** 1013
[30] Carcia A, Bianconi M and Natoli C R 1986 *J. Physique* **47** C8–49
[31] Moss S C and Newnham R E 1964 *Z. Kristallogr.* **120** 359
[32] Barriuso M T and Moreno M 1982 *Phys. Rev.* B **29** 2271
[33] Moreno M 1990 *J. Phys. Chem. Solids* **51** 835
[34] Moreno M, Arambura J A and Barriuso M T 1982 *Phys. Lett.* **87A** 307
[35] Henry M O, Larkin J P and Imbusch G F 1975 *Proc. R. Irish Acad.* **75** 97
[36] The transitions $^4A_2 \rightarrow {}^2E$ are magnetic dipoles since the intensity ratio is $I(R_1):I(R_2) \approx 4:3$ instead of 3:1 [35]
[37] Qiu Y 1993 *J. Phys.: Condens. Matter* **5** 2041
[38] It must be pointed out that there is an error in the calculation by Yu and Zhao [39] because D(observed) is $(-199 \pm 7) \times 10^{-4}$ cm^{-1} instead of $(34.5 \pm 5) \times 10^{-4}$ cm^{-1} [17, 40]. Adopting the CDP [21], we have obtained the bond length values of $R_\parallel = 2.09$ Å and $R_\square = 2.13$ Å for MnF_2, which are consistent with the structure data obtained by Baur [41] ($R_\parallel = 2.10 \pm 0.01$ Å; $R_\square = 2.13 \pm 0.02$ Å), which again supports the determination of the bond lengths through the optical and EPR measurements.

[39] Yu W L and Zhao M G 1987 *J. Phys. C: Solid State Phys.* **18** L1087
[40] Tinkham M 1956 *Proc. R. Soc.* A **236** 535
[41] Baur H W 1958 *Acta Crystallogr.* **11** 488